

Article

An Offshore Floating Wind–Solar–Aquaculture System: Concept Design and Extreme Response in Survival Conditions

Xiangyuan Zheng ¹, Huadong Zheng ^{1,2,*}, Yu Lei ^{1,2}, Yi Li ¹ and Wei Li ³

¹ Division of Ocean Science and Technology, Tsinghua University, Shenzhen International Graduate School, Shenzhen 518005, China; zheng.xiangyuan@sz.tsinghua.edu.cn (X.Z.); lei-y16@mails.tsinghua.edu.cn (Y.L.); liyi@sz.tsinghua.edu.cn (Y.L.)

² Department of Civil Engineering, Tsinghua University, Beijing 100084, China

³ Powerchina Huadong Engineering Corporation Limited, Hangzhou 311122, China; li_w@ecidi.com

* Correspondence: zhenghd18@mails.tsinghua.edu.cn

Received: 24 November 2019; Accepted: 18 January 2020; Published: 30 January 2020



Abstract: This study presents a new concept design combining multiple megawatt (MW) vertical-axis wind turbines (VAWTs) and a solar array with a floating steel fish-farming cage. This combined wind–solar–aquaculture (WSA) system is intended to utilize the ocean space and water resources more effectively and more economically, while greatly shortening the payback period of investment in offshore power generation. The details of this WSA design are described, showing that a square-shaped fishing cage serves as a floating foundation for the 7600 m² solar array and four multi MW VAWTs. The WAMIT program based on potential-flow theory is employed to obtain the WSA's motion response amplitude operators (RAOs) in sinusoidal waves of varying periods. The motion RAOs indicated that the proposed concept possesses better hydrodynamic seakeeping performances than its OC3Hywind spar and OC4DeepCwind semi-submersible counterparts. A potential site located in the northwest South China Sea is selected to deploy the WSA. Its feasibility is then examined in terms of the hydrodynamic motions and structural dynamic response driven by wind, waves, and current. Fully coupled time-domain simulations are carried out for 50-year survival conditions. The whole structure exhibits outstanding performance for its small motions in random wind and seas. Moreover, under these survival conditions, the top accelerations and tower base stresses of the VAWTs and mooring line tensions readily meet the design requirements. Technically, the WSA has strong competitiveness and wide prospects in the offshore industry for both power exploitation and marine aquaculture in intermediate and deep waters.

Keywords: floating foundation; vertical-axis wind turbines; steel fish farming; combined solar–wind–aquaculture system; hydrodynamic analysis; survival conditions

1. Introduction

In order to reduce the massive greenhouse gas emissions from conventional fossil fuels and ensure energy sustainable development, natural renewable energy exploitation is more needed than ever. Among all possible natural energy resources, wind and solar energies are considered as the most promising alternatives to fossil fuels. The offshore region is now in focus for these two energies. To date, the installation of bottom-fixed offshore wind turbines in less than 40 m shallow water is well established; however, construction, transport, and site installation of foundations account for approximately 50% [1] of the total development cost of an offshore wind farm. As the number of wind turbines employed in deeper waters is speedily increasing, this proportion rises significantly; thus, floating offshore wind turbines are a promising alternative for the offshore wind industry. On the other

hand, offshore aquaculture is also developing rapidly and moving into deeper and deeper waters to acquire better water resources. The Ocean Farm 1 fishing facility [2] is an outstanding milestone in the history of aquaculture for its unusual size of 122 m in diameter and for the steel frame never adopted before. These two fields, offshore aquaculture and offshore wind industry, seem irrelevant, whereas in reality they can be combined together to utilize the marine space resources more effectively.

For the last decade, floating horizontal-axis wind turbines (HAWTs) were a research focus in deep water wind power exploitation because of their successful application. The milestone Hywind Scotland pilot-park wind farm (5×6 MW) (2017), which is the world's first commercial floating wind energy project [3], also drove the further development of floating HAWTs. Since then, more studies on floating HAWTs emerged, mainly on foundation design, structural integrity, and installation, aiming at offering specific guidance to the structural design and reducing construction costs. Nevertheless, two main drawbacks may restrict the development of large-scale HAWTs in deeper-water regions. One is the heavy nacelle generator at high altitude, which not only demands costly marine operation and maintenance but also causes unfavorable instability and structural resonance. The other is the large separation distance required between any two HAWTs. Even if HAWTs are 3–5 turbine diameters apart in the cross-wind direction and 6–10 turbine diameters apart in the downwind direction, there is 10% performance loss due to the impacts of adjacent turbine wakes [4]. By contrast, vertical-axis wind turbines (VAWTs) have several advantages [5], such as a much lower center of gravity, much lower installation and maintenance costs, much lower noise, and a simpler power generation system. Although, compared with HAWTs, VAWTs have a relatively lower power coefficient, they can interact synergistically to enhance the total power production when placed in close proximity. It means that VAWTs can be installed in a cluster pattern on a single floating foundation. All these factors are in favor of the bright prospect of VAWTs for offshore power exploitation, which revived researchers' interest in floating VAWTs. Several pilot projects for floating VAWTs, such as the Vertiwind project [1], Deepwind project [6], and Aerogenerator X project [7], were developed, and their technical feasibilities were also evaluated.

For substructures, the floating foundation used to support a wind turbine can be classified into three main categories in terms of the mechanism of maintaining hydrostatic stability: tension leg platform (TLP) type [8], semi-submersible type [9–11], and spar type [12,13]. Site metocean conditions, fabrication, towing, and installation are all important factors that determine the foundation type. Although TLP was widely developed in oil and gas industry for many years, it has great challenges in terms of tendon installation, higher marine operation cost, and the change in tendon tension resulting from tidal variations [14]. The semi-submersible foundation is characterized by a large displacement and a large water plane area contributing to good hydrostatic stability. For instance, the WindFloat concept proposed by Roddier et al. [9] is a typical semi-submersible platform for floating wind turbines including three-legged fat columns and auxiliary water-entrapment plates providing additional damping forces. The spar foundation was extensively studied through numerical analyses [15,16] and experiments [17,18]. Due to its excellent hydrostatic stability and hydrodynamic performance, spar became the first commercialized floating foundation that was adopted by the Hywind Scotland wind farm, and it demonstrated very good performance in the North Sea severe environments since the end of 2017 [3]. As a matter of fact, none of the above-mentioned floating platforms make full use of the huge space created by the foundation, whereas this huge underwater space could be used for the aquaculture industry without compromising the efficiency of wind power generation and the dynamic performance of the floater. This philosophy, therefore, inspired the authors to conceive of a floating wind turbine foundation with a steel fishing cage, which is an attractive approach to significantly reduce the long payback period of floating wind turbines, while achieving the goal of fully utilizing the marine resources.

In addition to wind energy, solar energy is also recognized as one of the most viable renewable energy resources in the world. Nevertheless, wind and solar energy exploitations heavily depend on the weather [19]. Fortunately, the problem can be alleviated to a large extent by integrating the two energies into a complementary manner with respect to time blocks and space [20,21]. So far, almost no offshore structures were developed to effectively accommodate solar panels in a harsh ocean

environment due to a costly investment on the substructure (either fixed or floating). If the foundation has a large area to accommodate the solar array, the total capacity of wind and solar power generation can be increased, and it becomes more constant.

In this study, a novel concept that combines multiple megawatt (MW) vertical-axis wind turbines (VAWTs) and a solar array with a floating steel fish-farming cage is proposed. Four VAWTs are mounted on the corner columns of a square steel fishing cage in a compact pattern while meeting the minimum neighboring proximity requirement. The solar array, as large as 7600 m², is installed on the top of the cage, forming a system complementary to wind energy generation. The steel fishing cage not only works for fish cultivation but also serves the top structure (including VAWTs, solar array, and living quarters) as a floating foundation. The whole system is designed to be unconditionally stable with its center of gravity (CG) lower than center of buoyancy (CB). The potential theory and Morison formula accounting for wave actions are applied for hydrodynamics. The seakeeping performance of the structure is compared against the currently popular OC3Hywind spar [22] and OC4DeepCwind semisubmersible wind turbines [23]. As a case study, a potential offshore site located in the northwest South China Sea is selected for this new conceptual offshore structure to examine its feasibility in terms of hydrodynamic and structural performance. The extreme responses under a 50-year wave and wind condition are investigated using software OrcaFlex (v10.3c, Orcina, Cumbria, UK) [24].

2. The WSA Concept

As shown in Figure 1a, the WSA concept comprises five main parts: (1) a multi-function steel fishing cage, (2) four VAWTs, mounted on the cage for capturing wind energy, (3) a solar array for capturing solar energy, (4) spread catenary moorings for station keeping, and (5) living quarters for personnel accommodation. This concept is a combined wind–solar–aquaculture system (WSA), aiming at utilizing the limited marine space and ambient water resources more economically and effectively. The estimated water volume inside the fishing cage exceeds 300,000 m³, which enables this hybrid system to produce a revenue of tens of millions of dollars solely from fish production. Hence, the payback period of the heavy investment in offshore wind power generation can be greatly reduced to several years. In turn, the power generated by the wind–solar system easily satisfies the electricity consumption by fishery.

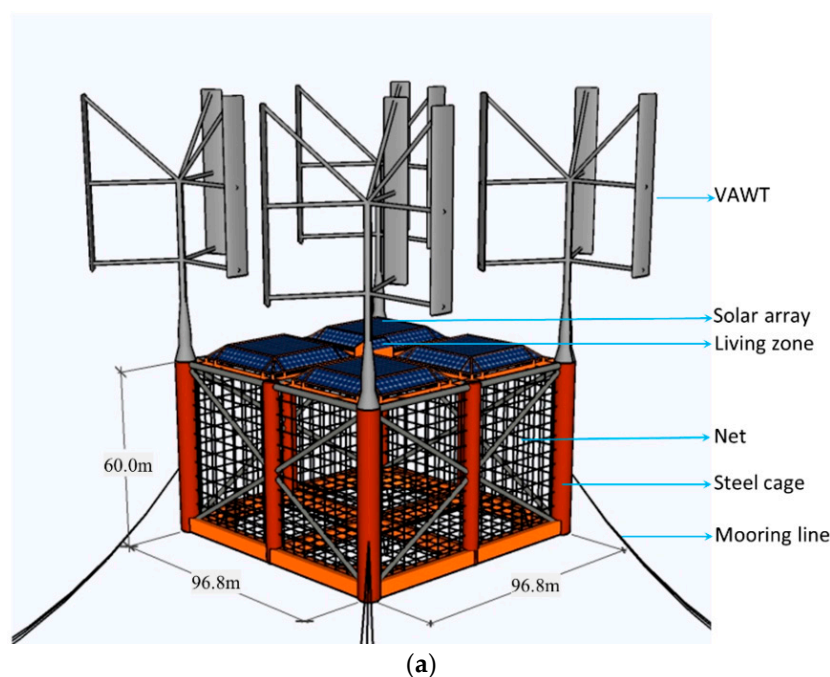


Figure 1. Cont.

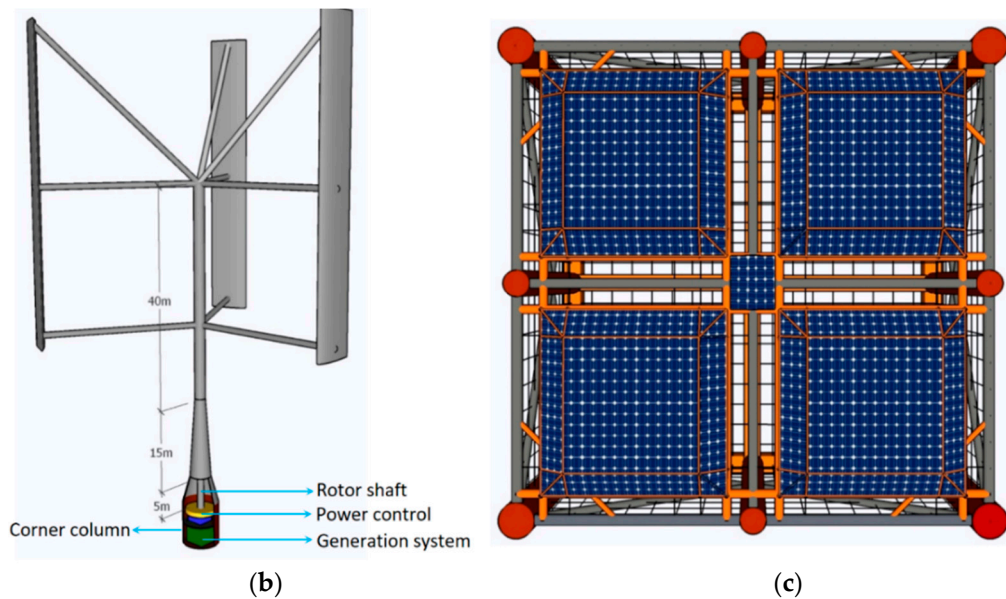


Figure 1. Concept of the wind–solar–aquaculture system (WSA): (a) perspective diagram of the WSA structure; (b) straight-bladed vertical-axis wind turbine (VAWT); (c) arrangement of the solar array—top view.

2.1. Steel Fishing Cage

For the design of an offshore engineering structure, water depth is always the most key parameter. The tentative and ambitious water depth to deploy a WSA ranges from 100 m to 200 m, which may cover humankind’s fish farming and offshore power exploitation activities for upcoming decades. The steel fishing cage consists of bottom rectangular pontoons, vertical cylindrical columns, and top and side cylindrical braces, as shown in Figure 2. The section details of cage structural members are given in Table 1. Stretched nets made of copper alloy are attached to all side frames and the bottom, forming a cage space (Figure 1). Because copper alloy nets have larger stiffness and suffer significantly lower drag forces than nylon nets [25], the stability of the cage volume is, therefore, enhanced. This is an advantage of the WSA when compared to the widely used high-density polyethylene (HDPE) cages. Moreover, compared to HDPE fishing cages, the steel fishing cage of the WSA system owns much higher strength and provides a much larger space for fishery. The contained effective water volume is approximately 315,000 m³, equivalent to 600 ordinary HDPE cages. In view of structural safety and the volume of fish production, like Ocean Farm 1, SWA greatly surpasses the traditional HDPE cages.

Table 1. Parameters for fishing cage structural members.

Member	Section (m)	Quantity	Length (m)	Thickness (m)
Bottom ring pontoon	B × H = 4.5 × 5.0	8	45.0	0.028
Bottom corner pontoon	B × H = 4.0 × 5.0	4	21.2	0.028
Bottom cross pontoon	B × H = 4.0 × 5.0	4	45.0	0.028
Corner column	D = 6.8	4	60.0	0.028
Central column	D = 5.0	1	60.0	0.028
Side column	D = 5.0	4	60.0	0.025
Side brace	D = 1.5	16	54.1	0.015
Top ring brace	D = 2.0	8	45.0	0.022
Top cross brace	D = 1.8	4	45.0	0.020
Top corner brace	D = 1.0	4	21.2	0.015

Notes: B: breadth; H: height; D: diameter.

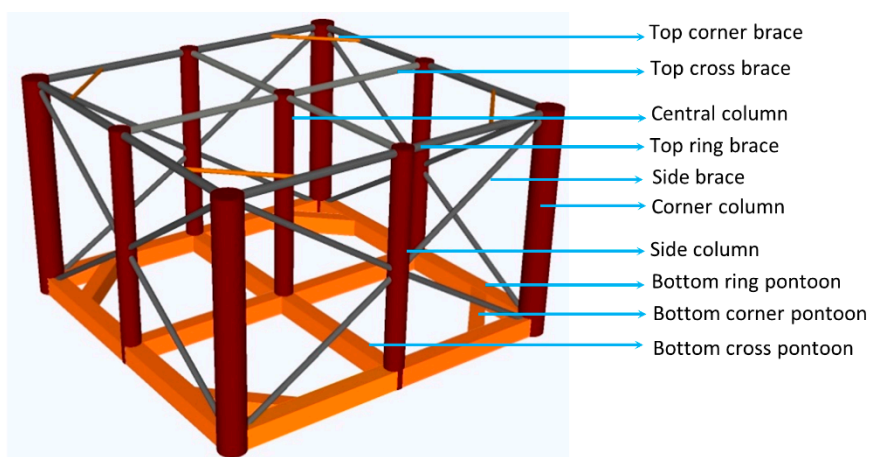


Figure 2. Steel fishing cage.

Use of the cage space for fishery is very flexible for the WSA. Four fishing zones can be partitioned with comparable dimensions to satisfy the cultivation of various fish species. The bottom fish nets can move up and down with an automatic lifting system in the cage for capturing fish with ease. Hence, the steel fishing cage serves a dual function, fish cultivation and the foundation for the wind turbines and solar array.

2.2. Wind–Solar Power System

According to the blade configuration, VAWTs can be classified into curve-bladed VAWT (Deepwind project), straight-bladed VAWT, V-shaped VAWT (Aerogenerator X project), and helical-bladed VAWT (Vertwind project). Among them, the curve-bladed floating VAWT [26] and the straight-bladed floating VAWT [27–29] were studied for a relatively longer time, especially in terms of their aerodynamic performance. Compared with the curve-bladed VAWT, the straight-bladed VAWT is more efficient, since the whole length of each straight blade can capture wind for power generation, while, in the curve-bladed VAWT, the upper and lower parts of each wing are used with a lower efficiency. Cheng et al. [29] studied the effect of blade number on the dynamics of floating straight-bladed VAWTs and concluded that the variation of tower base bending moment can be significantly reduced by increasing the number of straight blades from two to three. Therefore, the WSA system adopts three straight-bladed VAWTs evenly mounted on the steel fishing cage. The blade section is of symmetrical shape NACA-0018 [30]. Unlike the heavy nacelle generator at high altitude in HAWTs, the generation system of a VAWT is placed inside the main columns of the floating foundation so as to lower the CG as shown in Figure 1b. The design parameters for a rated power of 3 MW are listed in Table 2. The efficiency of overall power generation for all turbines is subject to their layout and the main incidence angle of wind. The wake effects are likely to lower the performance of downstream turbines. As this study is aimed at evaluating the feasibility of the new concept of the WSA, optimization of the layout is not within the scope of the present study.

Table 2. Main parameters of the wind–solar power generation system. VAWT—vertical-axis wind turbine; SWL—still water level.

VAWT	
Blade number	3
Blade height (m)	60
Chord length (m)	3
Aerofoil section	NACA-0018
Rotor Radius (m)	30
Total height measured from SWL	99

Table 2. Cont.

Cut-in, rated wind, cut-out wind speed (m/s)	5.0, 14.0, 23.0
Rated rotational speed (rad/s)	3.12
Weight for each VAWT (t)	350
Total weight (t)	1400
Rated power for each VAWT (MW)	3
Total rated power (MW)	12
Solar Array	
Weight of support truss (kg/m ²)	0.023
Weight of solar panels (kg/m ²)	0.033
Area of each zone (m ²)	1900
Total area (m ²)	7600
Total rated power (MW)	1.52

The solar array is fixed onto a truss structure as the roof of the steel fishing cage to capture solar energy. The array has four isolated zones as shown in Figure 1c. Each zone has an area of 1900 m² and is designed in a truncated square pyramid shape to reduce the wind load on array. Note that only the roof of the fishing cage is mainly covered by the solar array, while sufficient sunlight is guaranteed for aquaculture health. Weights of the solar array and support truss are given in Table 2. The solar array provides about 1.52 MW power generation, assuming a rated power of 200 W for 1 m² of solar panel.

2.3. Mooring System

The station keeping of the WSA and its pitch and roll rotations are vital to the dynamic stability of the structure. Rotation levels mainly rely on the WSA's inherent characteristics such as moment inertias and the relative distance between CG and CB, while the station keeping depends on the mooring system. In this study, catenary mooring lines rather than polyester lines are used for the following reasons:

1. Tendon tension in polyester lines significantly shortens the natural period of motion and makes the floater more sensitive to wave-frequency loads;
2. The water depth considered in the present study is 100–200 m in offshore continental shelves, where taut polyester lines are affected by tidal variations;
3. At the same water depth, use of polyester lines incurs a higher cost than catenary chains in installation and maintenance.

As shown in Figure 3, the WSA system is moored by 12 identical catenary lines deployed symmetrically around the fishing cage, following the design provisions in DNVGL-OS-E301 [31]. The planar angle between two neighboring lines in each spreading direction is 5°. Fairleads are located at the four main corner columns slightly above CB to further reduce the surge and pitch motions [32]. Several key design parameters of mooring lines are given in Table 3.

Table 3. System parameters.

Segment	Length (m)	Diameter (m)	Mass Density (kg/m)	Break Load (kN)	Characteristic Strength (kN)
Upper line	135	0.115	82.0	3965	3766
Lower line	507	0.115	82.0	3965	3766
Clump mass	8	0.930	11,666	-	-

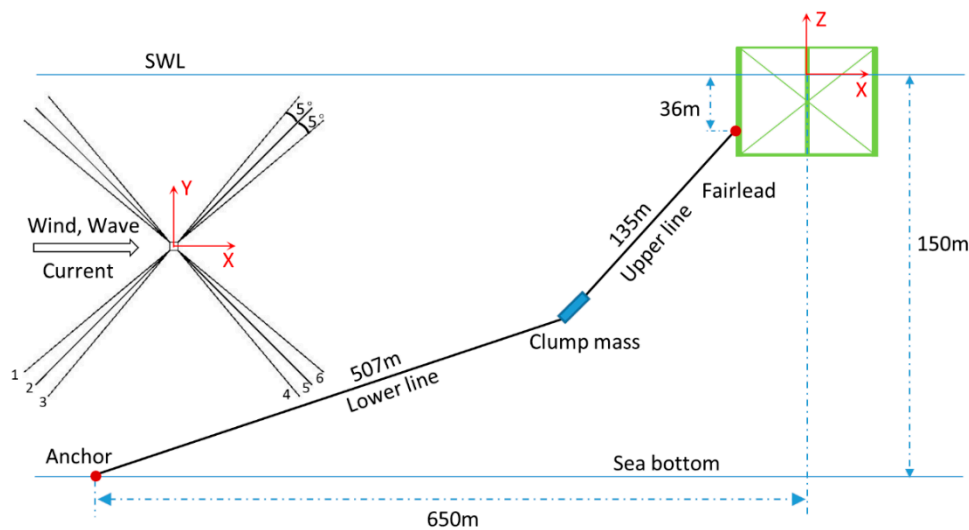


Figure 3. Mooring system layout.

2.4. Transport and Installation

The transport and installation costs of a floating offshore wind farm greatly depend on the design philosophy, which includes fabrication, assembly, and marine operation procedures [33]. Previous research [34] suggests that the logistics and installation cost of a floating wind farm account for some 19% of the total construction cost. In order to reduce the considerable site installation and operation costs, the proposed concept of the WSA allows pre-fabrication of the fishing cage in several modules and then assembly on the dock. It is followed that the dock installation of all VAWTs and the solar array can be readily accomplished before the WSA is transported to the desired offshore operation site. Thus, the heavy cost incurred by marine installation of towers and wind turbines can be saved.

The transport of the WSA to the operation site can be realized by wet tow using tugs (Figure 4) because the buoyancy provided by WSA is sufficient to balance its own weight and dead concrete ballast (See Table 4). The maximum transit draft is 10 m. At this transit draft, the righting moment versus heel angle is given in Figure 5, demonstrating good stability during wet tow. When the WSA reaches its operation site, the draft can be adjusted by water ballasted into pontoons and columns (Figure 6). The ideal operation draft is 51 m. Transit and operation states are illustrated in Figure 4.

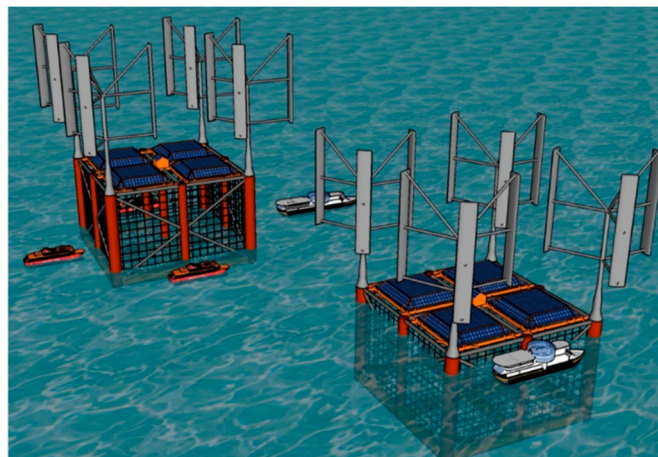


Figure 4. Transit and operation of the WSA.

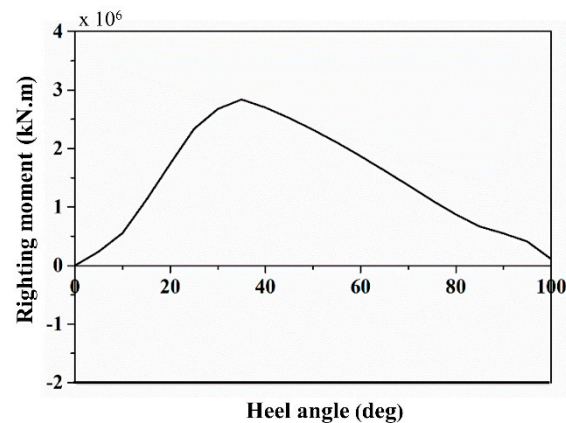


Figure 5. Stability curve of the WSA: righting moment vs. heel angles.

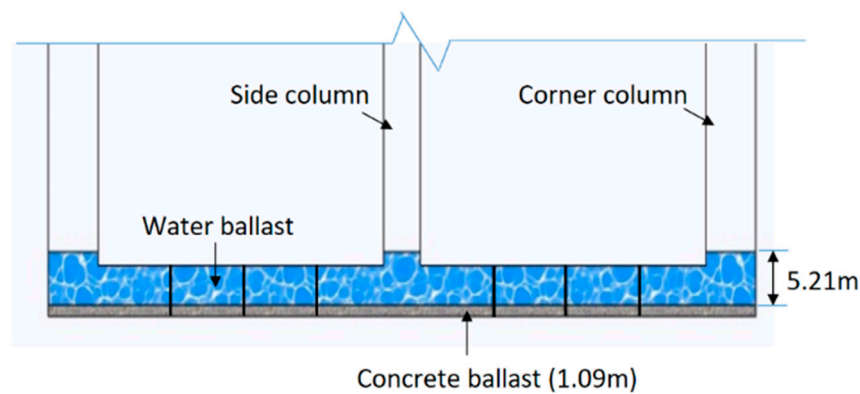


Figure 6. Ballast arrangement.

Table 4. Parameters of the wind–solar–aquaculture system (WSA) in static equilibrium position. CG—center of gravity; CB—center of buoyancy.

Item	Value
Total mass (excluding ballasts) (kg)	6.916×10^6
Dead concrete ballast (kg)	8.560×10^6
Water ballast (kg)	1.026×10^7
Towing displacement (m^3)	1.510×10^7
Operation displacement (m^3)	2.511×10^7
CG (m)	(0,0,-40.73)
CB (m)	(0,0,-36.23)
Transit draft (m)	10
Operation draft (m)	51
Volume net (m^3)	3.15×10^5

3. Hydrostatic Analysis of WSA

The hydrostatic analyses are for the structure at the static equilibrium position, where the buoyancy balances the overall weight of the system including wind turbines, solar array, steel fishing cage, nets, ballasts, and the mooring system. The relevant hydrostatic parameters in this status are given in Table 4. Ballasts are mainly placed in bottom ring pontoons, bottom corner pontoons, and side and corner columns to improve the moment of inertia of the structure as shown in Figure 6. Note that the Cartesian system defined in this study is that X and Y axes sit on the central column of the structure and Z is positive when measured upward from the still water level (SWL), as shown in Figure 3.

In WSA, the CG is 4.5 m below the CB, which means that the system is unconditionally stable like a spar-type floater. In calm water, the finite element software ABAQUS (v14.0, DASSAULT SYSTÈMES,

Paris, France) [35] is used to analyze the steel cage under gravity and buoyancy. The structural members are modeled with beam elements. The four wind turbines, the solar array (four zones), and the living quarters are simplified as lumped masses, and the ballast mass is evenly shared onto the adjacent element nodes in the finite element model. Buoyancy forces on pontoons and columns are modeled as uniformly distributed loads on their undersurfaces. Figure 7 illustrates the deformation of the steel cage. For such a megastructure, the largest deformation of only 112 mm occurs at the connection of the center column and bottom cross pontoons. This is because most of the ballasts are evenly distributed at the bottom ring pontoons, while weight and buoyancy are not balanced at the center part, such that very slight hogging deformation appears. In order to investigate the dynamic property of the steel cage itself, the three translational degrees of freedom (DOFs) are restricted at fairleads. The first three vibration modes of the cage are shown in Figure 8. It is demonstrated that the smallest natural frequency of the cage itself is 0.81 Hz, far away from the frequency range (0.05–0.2 Hz) of primary ocean waves and wind frequencies (usually <math><0.01\text{ Hz}</math>). Hence, like many research works, it is reasonable to treat the steel cage as a rigid body in the hydrodynamic seakeeping analysis.

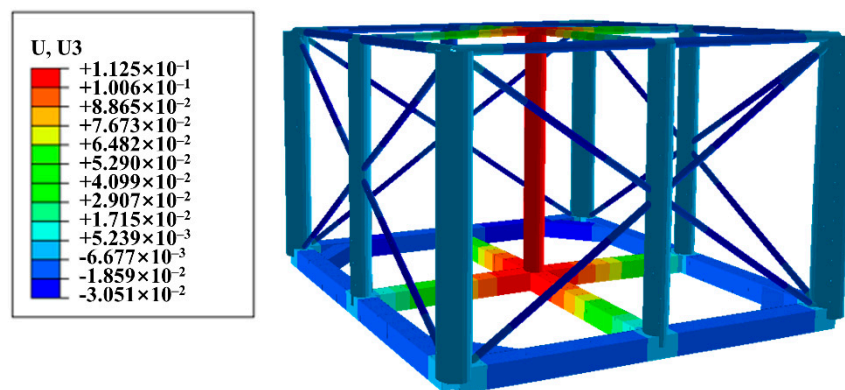


Figure 7. Deformation of the cage in calm water (unit: m).

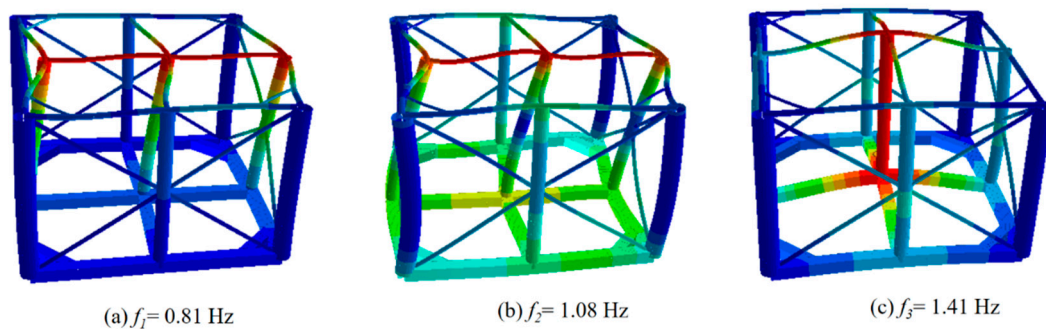


Figure 8. Natural modes and frequencies of the steel cage.

4. Hydrodynamic Analysis of WSA

4.1. Hydrodynamic Modeling of Foundation

The hydrodynamic performance of the WSA is investigated using the frequency-domain program WAMIT [36] that was developed based on the potential-flow theory. Software MultiSurf (-v8.5, AeroHydro Inc, ME, USA) [37] is used in advance to create the geometry model of steel cage below the SWL. In modeling, the geometric symmetry is utilized such that only one-quarter of the steel cage needs to be handled. Then the wetted surfaces of the WSA shown in Figure 9 are exported to WAMIT for the hydrodynamic analysis with sinusoidal waves of varying periods. In the linear WAMIT analysis, the effect of irregular frequencies is removed by manually paneling the free surface, and the higher-order method is applied to improve the calculation accuracy.

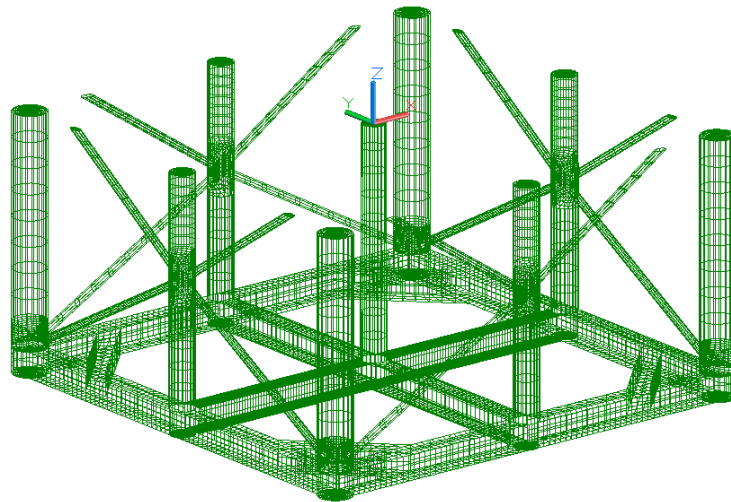


Figure 9. Wetted surface model in MultiSurf.

4.2. Response Amplitude Operators and Natural Periods of WSA

The response amplitude operator (RAO) is a normalized response function represented by the ratio of the floater's motion amplitude to the amplitude of incident sinusoidal wave. As one of the most important hydrodynamic characteristics of a floating structure, the motion RAOs of the WSA are calculated and compared to its counterparts OC3Hywind spar concept [22] and OC4DeepCwind semi-submersible concept [23]. By applying Newton's law, the amplitudes of the cage floater's six-DOF motions x (ordered as surge, sway, heave, roll, pitch, and yaw) can be obtained by solving the following 6×6 linear system:

$$[-\omega^2(M + A) + i\omega(B + B^E) + (C + C^E)]x = F_{Exc}, \quad (1)$$

where M is the inertia matrix of the WSA system, A is the added mass matrix, B is the radiation damping matrix, B^E is the external damping matrix, C is the hydrostatic and gravitational restoring matrix, C^E is the external stiffness matrix when the mooring system exists, and F_{Exc} is the vector of the wave excitation force in the directions of the six-DOF motions. Note that in WAMIT, A , B , and C are firstly solved by the subprogram POTEN, and then F_{Ext} is calculated by the subprogram FORCE.

The damping in Equation (1) produces significant effects on the floater's response. However, the added damping matrix B from WAMIT only considers the radiation damping resulting from the oscillation of the steel cage in waves. Due to the fact that there are fish nets and a large number of slender members in the substructure of the WSA, the viscous drag damping induced by flow separation [14] is more significant than the radiation damping and must be taken into account for the hydrodynamic analysis. Therefore, an external liner damping matrix, B^E , is introduced into WAMIT. B^E only contains diagonal elements that are as follows:

$$[B^E]_{ii} = 2\xi_i(M_{ii} + A_{ii})\left(\frac{2\pi}{T_i}\right), \quad i = 1, 2, \dots, 6, \quad (2)$$

where ξ_i is the equivalent damping ratio in the i -th DOF, and the natural period T_i is obtained from the free decay test (see Table 5).

In this study, the free decay tests are carried out using the software OrcaFlex [24]. This tool is a fully nonlinear finite element software, able to compute wave forces on and displacements of fish nets. Since OrcaFlex is unable to calculate the wave load on slender rectangular-shaped members, equivalent cylindrical members are used to substitute them with equivalent drag coefficients, as shown in Figure 10. The drag coefficients C_d for equivalent cylindrical members can be obtained through linear interpolation of the results by Barltrop [38]. In order to improve the calculation efficiency, modeling of fish nets is also simplified on the basis of the principle that the projected area and wet

mass of the netting material are identical between the model and the prototype [39]. The numerical model in OrcaFlex for hydrodynamic calculation involving VAWTs and the solar array is shown in Figure 10. To verify the WSA model in OrcaFlex, the floater's responses under an Airy wave (wave period of 12 s and wave height of 4 m) are calculated and then compared against FAST (Fatigue, Aerodynamics, Structures, and Turbulence) [40]. Figure 11 illustrates the calculated surge, heave, and pitch motions. It is noticeable that there are good agreements between the results of these two widely used programs. Based on the validated model, the natural periods and damping ratios of the six DOFs obtained from the numerical free decay tests are listed in Table 5. Note that, as the WSA is nearly symmetrical about both X and Y axes, surge and sway motions have the same natural periods, as well as pitch and roll motions.

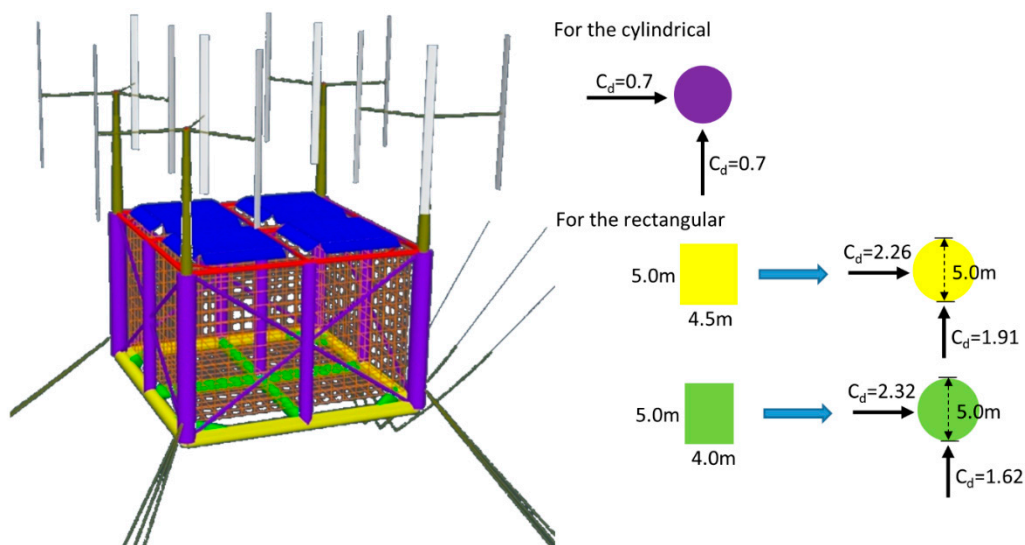


Figure 10. Numerical model and equivalent drag coefficients for the parked condition of turbines.

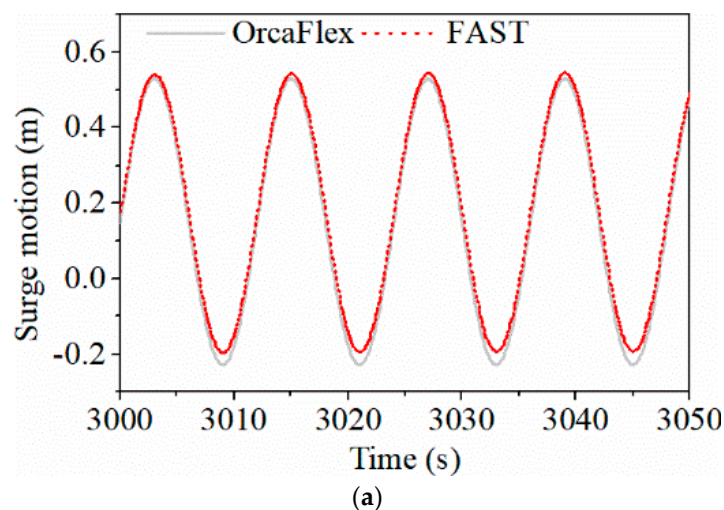


Figure 11. Cont.

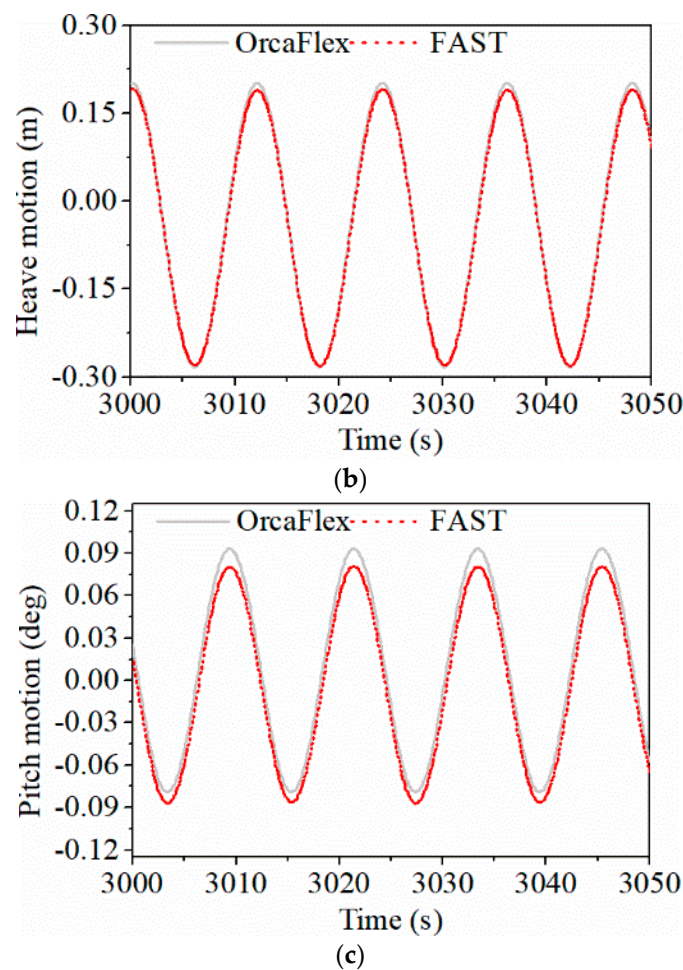


Figure 11. Comparison of WSA motions: OrcaFlex vs. FAST. (a) Surge motion; (b) Heave motion; (c) Pitch motion.

For the freely floating state, Figure 12a,b respectively compare the heave and pitch RAOs of the WSA system to the currently most favorable offshore wind turbine concepts (OC3Hywind and OC4DeepCwind) in head seas. It can be observed that the periods of the WSA corresponding to the peak heave and pitch RAOs, 25.2 s and 23.0 s, are far beyond the most possible wave period range of 5–20 s, indicating that its motions are insensitive to wave-frequency hydrodynamic loads. By contrast, the large heave motion of OC4DeepCwind could be triggered by long high sea waves in that the corresponding natural period of heave is located at 17.5 s. The heave peak value of WSA is 3.8 m, only slightly higher than that of the OC3Hywind concept. Moreover, it can be seen that the peak pitch RAO of WSA is only 1.3° , much smaller than the other two concepts. For the usually encountered wave period $5\text{ s} < T < 20\text{ s}$, the pitch RAOs of WSA are all lower than those of OC3Hywind. Thus, in general, the hydrodynamic seakeeping performance of the WSA outperforms its counterparts OC3Hywind and OC4DeepCwind. There are two reasons to explain this good characteristic of WSA, one is its remarkably larger displacement than OC3Hywind and OC4DeepCwind, and the other is its significantly larger dimensions in length and width that produce a greater moment of inertia for small pitch and roll. On the contrary, for example, the substructure of OC3Hywind is actually a single column [22]. Furthermore, comparing the peak heave and pitch periods in Figure 12 with those in Table 5, it can be noticed that the catenary mooring system and fish nets in the WSA bring negligible change on the natural periods.

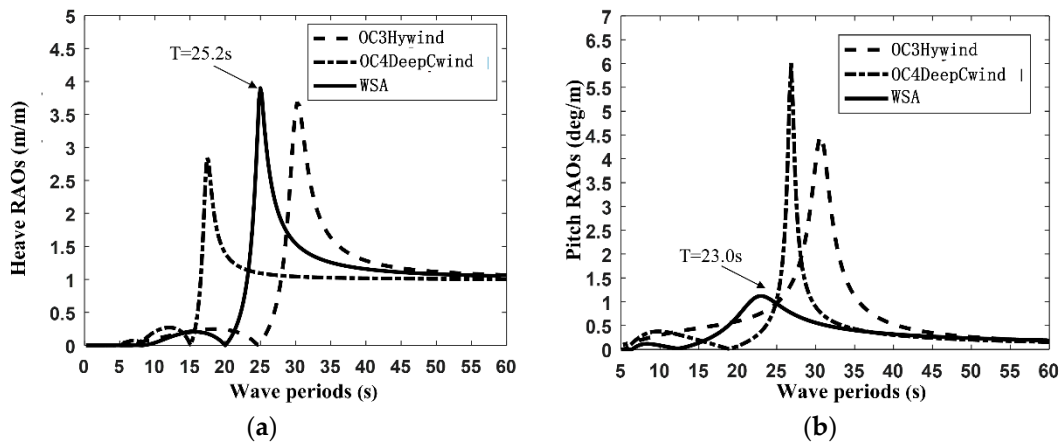


Figure 12. Comparisons of motion response amplitude operators (RAOs) in freely floating states. (a) Heave; (b) Pitch.

Table 5. Natural periods and equivalent damping ratios of the WSA rigid body motions.

Motion	Natural Period (s)	Natural Frequency (Hz)	Equivalent Damping Ratio (%)
Surge/Sway (s)	89.9	0.011	3.51
Heave (s)	25.4	0.039	2.59
Pitch/Roll (s)	23.2	0.043	2.00
Yaw (s)	55.4	0.018	3.88

5. Stochastic Response of WSA

5.1. Governing Equation of Motions in Time Domain

The foregoing section only tackled the WSA's rigid-body motion under sinusoidal ocean waves in the frequency domain, where the steel cage is only subjected to idealized waves. In real sea environments, WSA is subjected to random waves, current, and wind. Not only the cage's motions but also wind turbine structural responses are stochastic in nature. Furthermore, they are coupled in multi-body dynamics, as the wind tower, for instance, is a flexible structure. Calculation of such a coupled dynamic response has to be handled in the time domain as in the following equation:

$$(M + A_{\infty})\ddot{x} + \int_{-\infty}^{+\infty} \kappa(t - \tau)\dot{x}d\tau + (C + C^E)x = F_{Wave} + F_{Drag} + F_{Current} + F_{Wind}. \quad (3)$$

This is the so-called Cummins equation [41] involving the retardation function $\kappa(t - \tau)$ to account for the frequency-dependent added mass and radiation damping, x is the six-DOF cage motions, and A_{∞} is the added mass matrix of the steel cage at high frequencies. F_{Wave} is the wave exciting force from potential flow theory, F_{Drag} and $F_{Current}$ are the drag force (Equation (4)) and current force on submerged cage members and fish nets, noting that the current has a linear decay profile from SWL and downward [42], and F_{Wind} consists of three parts (Equation (5)): wind lift force f_l on blades (Equation (6)), drag force f_d on blades (Equation (7)), and drag forces f_D (Equation (8)) on the towers, struts, and solar array.

$$F_{Drag} = \frac{1}{2}\rho_w A C_d (u - \dot{x})|u - \dot{x}|, \quad (4)$$

$$F_{Wind} = f_l + f_d + f_D, \quad (5)$$

$$f_l = \frac{1}{2}\rho C_L(\alpha) A v^2, \quad (6)$$

$$f_d = \frac{1}{2}\rho C_D(\alpha) A v|v|, \quad (7)$$

$$f_D = \frac{1}{2} \rho C_{D1} S v |v|, \quad (8)$$

where ρ_w , A , C_d , and u in Equation (4) are the water density, area of members inside the fluid, drag coefficient for members inside the water, and the water particle velocity, respectively. The values of C_d are shown in Figure 10. ρ , S , and v in Equations (6)–(8), are the air density, projected area, and relative wind velocity, respectively. $C_L(\alpha)$ and $C_D(\alpha)$ are the lift coefficient and drag coefficient for airfoils, dependent on the incident angle α . For the wind load on the towers, struts, and solar array, Equation (8) is used. This equation involves the drag coefficient C_{D1} . For towers and struts, $C_{D1} = 1.17$ [43], while, for the solar array, C_{D1} on every facet of the truncated pyramid is determined by the design code [44], as depicted in Figure 13. Note that minus signifies pressure acting away from the upper surfaces.

The present study is aimed at evaluating the dynamic response of WSA under survival conditions, in which the turbines are in parked status. The aerodynamic loads and induced responses for the turbine operational condition will be discussed in a further study. In the design for structural safety, it is very important to fathom the extreme dynamic responses. For the ultimate limit state that is associated with structural strength in design, design codes and standards [45] specify a number of critical load cases combining wind and wave effects. The 50-year design wave and winds are chosen to examine the technical feasibility of the WSA.

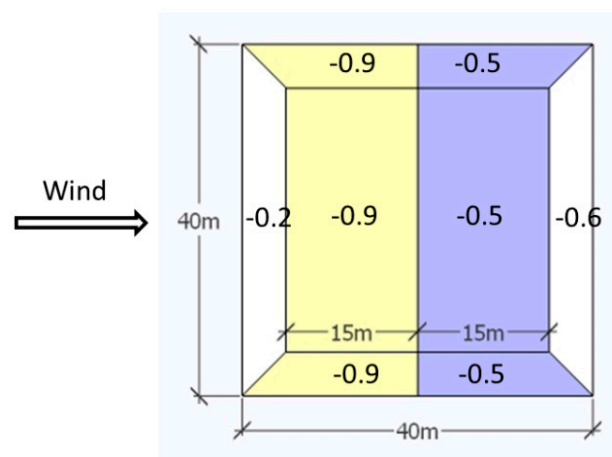


Figure 13. C_{D1} for wind loads on facets of a zone of solar array.

5.2. Wind and Wave Statistics

Guangdong province of China is a regional pioneer and leading investor in offshore renewable energy exploitation and fishery industries. As shown in Figure 14, a potential offshore site to deploy the WSA is located at 118.1° east (E) and 22.0° north (N). It is about 87 km off the coast, and the water depth is 150 m if storm surge and astronomical tide are both counted. The local wind resource is abundant, classified as level A in China. Sea water there is in favor of marine aquaculture for the warm water even in winters and a wide variety of planktons and algae.

In this study, site wind and wave conditions rely on the dataset provided by the European Center for Medium-Range Weather Forecasts (ECMWF) [46]. This set of data including mean wave periods T_1 , significant wave heights H_s , and 10-min mean wind speeds at height 10 m U_{10} are available online for 40 years, from 1979 to 2018, with a time resolution of 6 h. For each variable, as many as 58,440 discrete samples are extracted and then statistically processed to determine the wave and wind conditions.

The Pierson–Moskowitz (PM) spectrum [42] and API spectrum [47] are selected to respectively describe wave and wind conditions. Peak wave period T_p and H_s fully specify the Pierson–Moskowitz spectrum, while the height above the SWL and U_{10} can define the API spectrum at a specific altitude. It is assumed that the exponent of the wind profile is 0.11 and the turbulence intensity is 11% [48]. The

annual extremes of environmental variables, such as H_s and U_{10} , are assumed in the form of a Gumbel distribution [42], i.e.,

$$F(x) = \exp\left\{-\exp\left[-\left(\frac{x-b}{a}\right)\right]\right\}, \tag{9}$$

where a and b are Gumbel distribution parameters that can be fitted from the annual maximum significant wave heights and wind speeds shown in Figure 15. Based on Equation (9), for the 50-year return period, $H_s = 8.62$ m and $U_{10} = 23.70$ m/s are derived for the design condition.

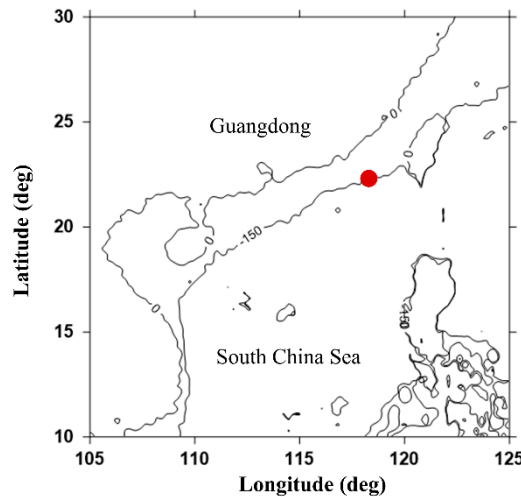


Figure 14. The hypothetical deployment site of the WSA.

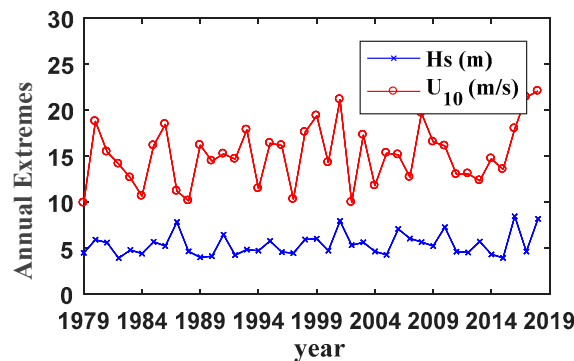


Figure 15. Maximum significant wave height H_s and wind speed U_{10} by years.

In order to determine the peak wave period T_p that is associated with H_s , the conditional modeling approach by Bitner-Gregersen and Haver [49] is used. T_p depends on the zero-crossing wave period T_z which is modeled by a lognormal distribution with H_s as follows:

$$f_{T_z|H_s}(t|h) = \frac{1}{\sigma t \sqrt{2\pi}} \exp\left\{-\frac{(\ln(t) - \mu)^2}{2\sigma^2}\right\}, \tag{10}$$

$$\mu = E[\ln T_z] = a_0 + a_1 h^{a_2}, \tag{11}$$

$$T_p = 1.4049T_z, \quad T_1 = 1.0867T_z, \tag{12}$$

where the distribution parameter μ is a function h , and $a_0 = 1.6192$, $a_1 = 0.1065$, and $a_2 = 0.9193$ can be calibrated based on the measurement data in Table 6; T_1 is the mean wave period. Then, Equations (10)–(12) yields the expectation of $T_p = 15.34$ s on the conditional level of $H_s = 8.62$ m. Table 7 lists three load cases (LCs). LC1–LC2 combining 50-year design waves and winds [45] are used to evaluate

the extreme responses of the WSA. In order to account for the swell-dominated sea for the site, the double-peaked (DP) Torsethaugen spectrum [50] is adopted in LC3 as shown in Figure 16, in which the swell period is specified at 25 s, very close to the natural periods of cage motions (Table 5). Note that LC1 and LC2 are wind–wave-dominated, whereas LC2 additionally considers a 50-year current speed of 2.05 m/s which is taken from Reference [31] for the South China Sea in tropical cyclones. LC1–LC3 are considered as survival conditions of the WSA, in which the wind speeds all exceed the cut-out wind speed of VAWTs. Thus, the VAWTs are also supposed to be parked without rotations. All blades in this situation are subject to lift and drag wind forces (Equations (6) and (7)). Each blade has a constant wind incident angle α throughout the whole duration of the time-domain simulation.

Table 6. Scatter diagram of H_s and T_z .

H_s (m) \ T_z (s)	3.5	4.5	5.5	6.5	7.5	8.5	9.5	10.5	11.5	Sum
0.5	0	5	89	33	0	0	0	0	0	127
1.5	31	4710	15,493	9563	2657	440	103	42	16	33,068
2.5	0	156	6249	9195	2030	496	151	73	35	18,392
3.5	0	0	48	3030	2270	276	82	40	4	5750
4.5	0	0	0	10	661	231	29	9	4	950
5.5	0	0	0	0	3	81	22	6	0	112
6.5	0	0	0	0	0	8	29	4	0	41
Sum	31	4871	21,899	21824	7621	1532	422	181	59	58,440

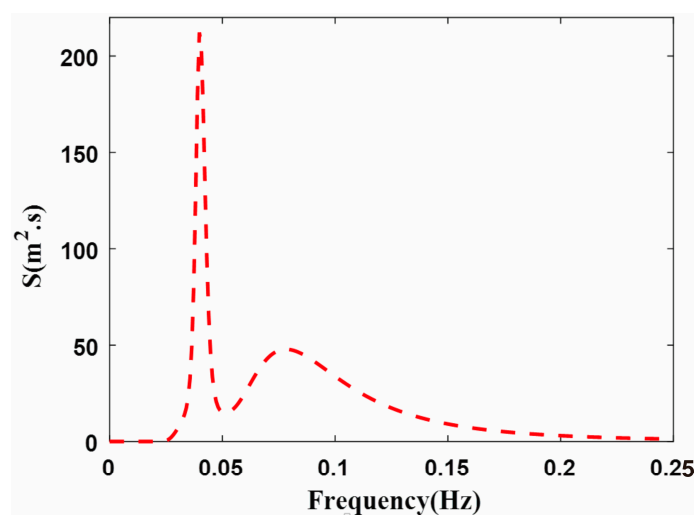


Figure 16. Double-peaked wave spectrum for load case 3 (LC3).

Table 7. Load cases (LCs). PM—Pierson–Moskowitz; DP—double-peaked Torsethaugen spectrum.

Load case	Spectrum		U_{10} (m/s)	H_s (m)	T_p (s)	Surface Current Speed (m/s)	Wind Turbine
	Wave	Wind					
LC1	PM	API	23.72	8.62	15.34	0	Idling
LC2	PM	API	23.72	8.62	15.34	2.05	Idling
LC3	DP	API	23.72	8.62	25.00	0	Idling

5.3. Extreme Analysis in Survival Conditions

5.3.1. Wind–Wave–Current-Induced Motion Responses

OrcaFlex [24] is adopted in this study to carry out the dynamic response analysis of the WSA system. In Figure 3, the directions of wind, waves, and current are assumed collinear to cause the most

severe dynamic motions and responses [29]. Time-domain simulations are carried out for a storm of 3-h duration. In the responses, the first 500-s time histories are truncated for the sake of transience.

Subjected to load cases LC1–LC3 in Table 7, the surge, heave, and pitch motions of WSA are calculated. Their statistics are shown in Table 8. Due to wind action, the mean surge in all three load cases is nonzero. As LC2 further considers the surface current speed of 2.05 m/s, the mean surge excursion reaches 10.88 m, which is about 3.7 m (or 50%) larger than that in LC1 and LC3. This indicates that, in addition to the wind, sea current is also a great factor influencing the surge excursion of the WSA and brings a new challenge to station keeping. The maximum surge of 15.38 m is about 10% of water depth, lower than the allowable offset limit of 12.5% [51]. The maximum pitch and heave motions occur in LC3, with 4.98° and 3.55 m, respectively. This is due to pitch and heave resonances that are induced by swell, whose period is assumed to be very close to the natural periods. However, LC3 is nearly an unrealistic load case because swell of that large H_s and T_p rarely happens in seas. Even so, the WSA system easily meets the requirement that maximum pitch motion must be less than 15° during non-operational load cases [52]. The mean heave motions are about 1.0 m in all LCs, due to the wind lift forces on the solar array. The small extreme heave and pitch motions in Table 8 demonstrate that the WSA system owns outstanding hydrodynamic performance. Therefore, variation in the incident angle of solar radiation, due to the WSA's oscillation, is also very small and causes negligible loss in solar energy production. Moreover, it can be seen that the skewness (the third standardized central moment) of heave and pitch motions in all load cases is no more than 0.1, and the kurtosis (the fourth standardized central moment) ranges from 2.9 to 3.2, except pitch motion in LC2, which is mainly driven by low-frequency swell. Thus, it can be revealed that the response of WSA tends to be Gaussian (i.e., in theory, skewness = 0 and kurtosis = 3) if the linear potential theory is applied to calculate the main hydrodynamic load on the floating foundation.

Table 8. Statistics of WSA motions.

Response	Statistics	LC1	LC2	LC3
Surge (m)	Max	11.49	15.38	11.85
	Min	2.55	7.64	2.67
	Mean	7.18	10.88	7.26
	SD	1.32	1.10	1.35
	Skewness	−0.01	0.42	0.01
	Kurtosis	2.87	3.24	2.91
Heave (m)	Max	2.89	2.75	3.55
	Min	−0.94	−0.63	−1.37
	Mean	0.99	1.01	0.96
	SD	0.51	0.46	0.75
	Skewness	−0.03	−0.01	−0.05
	Kurtosis	3.19	3.09	2.90
Pitch (°)	Max	2.48	2.35	4.98
	Min	−1.05	−1.00	−3.41
	Mean	0.70	0.65	0.69
	SD	0.50	0.49	1.48
	Skewness	−0.10	0.08	0.02
	Kurtosis	2.94	2.97	2.40

Note that skewness and kurtosis have no units.

The statistics of top horizontal acceleration (a_x), top vertical acceleration (a_y), and the bending stress at the tower base of a VAWT are listed in Table 9 for LC3. The extreme acceleration of 1.81 m/s² is below the design requirement of 0.6 g [52], and the extreme stress of 146 MPa is still within the elastic range of steel. The skewness and kurtosis of accelerations and stress in Table 9 again reveal that the non-Gaussian level of structural dynamic responses is weak. Thus, from the seakeeping and structural dynamic views, the WSA concept is a very promising and competitive candidate in the offshore industry.

Table 9. Statistics of horizontal and vertical accelerations (a_x , a_y) and tower base stress of a VAWT in LC3.

Response	Max	Min	Mean	SD	Skewness	Kurtosis
a_x (m/s ²)	1.81	−2.27	0.00	0.51	−0.05	2.95
a_y (m/s ²)	0.42	−0.46	0.00	0.12	0.00	2.83
Stress (MPa)	146.13	9.09	63.62	17.1	0.13	3.08

Note that skewness and kurtosis have no units.

Figure 17a illustrates the power spectra of surge motions in three design load cases. It can be seen that, in LC1 and LC2, noticeable spectral peaks appear at surge natural frequency ($f_{\text{surge}} = 0.011$ Hz in Table 5) and the dominant wave frequency ($f_{\text{wave}} = 1/T_p = 0.065$ Hz, $T_p = 15.34$ s in Table 7), while, in LC3, a sharp peak also appears at swell frequency ($f_{\text{swell}} = 1/T_p = 0.04$ Hz, $T_p = 25$ s in Table 7). The spectral peak at about f_{surge} is highest, mainly due to the low-frequency wind load. At f_{surge} , the peak value in LC2 is significantly lower than that in LC1 and LC3. This can be explained by the presence of current in LC2, which reduces the variation of surge motion at this low frequency. As illustrated in Table 8, the standard deviation of surge 1.10 m in LC2 is smaller than 1.32 m in LC1 and 1.35 m in LC3. Also, because surge and pitch motions are essentially coupled, pitch motion contributes to the overall surge to some extent. Therefore, for motion spectra (LC1 and LC2) in Figure 17a, there is a small peak at the pitch natural frequency ($f_{\text{pitch}} = 0.043$ Hz in Table 5). However, for LC3, the sharp peak at f_{swell} is attributed to the proximity between f_{swell} (0.04 Hz) and f_{pitch} (0.043 Hz).

For the power spectra of pitch and heave motions shown in Figure 17b,c, the spectral peaks are located at two frequencies. One is heave/pitch natural frequency ($f_{\text{heave}} = 0.039$ Hz, $f_{\text{pitch}} = 0.043$ Hz in Table 5), and the other one is located at the dominant wave frequency f_{wave} . Note that, in LC3, f_{swell} is very close to f_{pitch} and f_{heave} . Thus, the corresponding spectral peak amplitude is much higher than that in LC1 and LC2. By contrast, the peak values at f_{wave} are comparable to each other. Once again, it is illustrated in Figure 17b,c that existence of current helps to reduce heave and pitch motions, if the spectral peaks at natural frequencies are compared between LC1 and LC2. This reduction also agrees with quantities in Table 8 in which the standard deviation of heave in LC2 is slightly lower than that in LC1 (0.46 m vs. 0.51 m), as well as for the standard deviation of pitch (0.49° vs. 0.50°). As LC1 and LC2 are realistic extreme environmental sea conditions, the small spectral amplitudes in Figure 17a–c corresponding to these two load cases again exhibit excellent seakeeping performance under 50-year survival conditions.

5.3.2. Tension in Mooring Lines

The statistics of mooring chain tensions at fairlead and anchor in mooring lines 1–6 (Figure 3) are listed in Table 10 for LC2 whose surge motions are largest among all three load cases. The maximum and mean values of lines 1–3, as well as lines 4–6, are very close to each other, which suggests that the spreading direction of 5° does not lead to significant variations between neighboring mooring lines, and this is beneficial to station keeping of the system. When line 2 and line 5 are compared, it can be noticed that the mean fairlead tension in line 2 is 20% higher and the mean anchor tension is 38% higher. This is because lines 1–3 are windward, while lines 4–6 are leeward. The SD-to-mean ratios at fairlead and anchor in line 2 are 3.39% and 4.72%, respectively, larger than their counterparts of 2.11% and 3.51% in line 5, implying that the tension variation in line 2 is more significant, also because of the windward effect. When comparing the fairlead tension and anchor tension in the same mooring line, it can be seen that the fairlead tension is always larger by some 400 kN. Such tension reduction comes from seabed frictions, which is helpful to the seabed anchor design. More importantly, considering the partial safety factors 1.4 for mean tension and 2.1 for dynamic tension [31], the nominal extreme tension is as follows:

$$T_{\text{extreme}} = 1.4T_{\text{mean}} + 2.1(T_{\text{max}} - T_{\text{mean}}) = 3452 \text{ kN}, \quad (13)$$

which is safely below the characteristic strength of 3766 kN (Table 3).

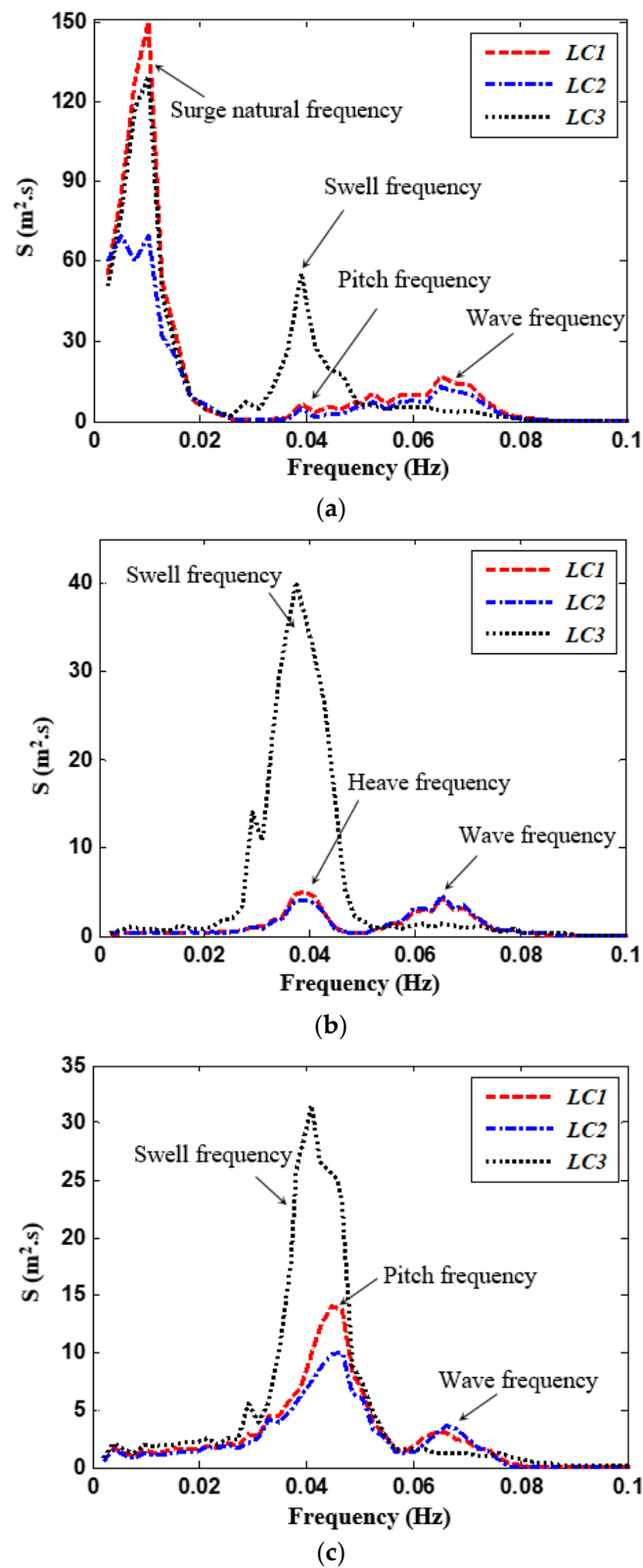


Figure 17. Response power spectra of WSA motions in three load cases: (a) surge; (b) heave; (c) pitch.

Table 10. Fairlead and anchor point tension statistics in LC2.

	Fairlead (kN)				Anchor (kN)			
	Max	Mean	SD	SD/Mean (%)	Max	Mean	SD	SD/Mean (%)
Line1	2262	1854	69	3.72	1846	1465	75	5.12
Line2	2190	1825	62	3.39	1760	1419	67	4.72
Line3	2179	1815	57	3.14	1739	1402	62	4.42
Line4	1683	1543	32	2.07	1218	1058	35	3.31
Line5	1657	1514	32	2.11	1191	1026	36	3.51
Line6	1667	1514	35	2.31	1205	1028	24	2.33

6. Conclusions

An innovative concept design of a floating WSA system that integrates four vertical-axis wind turbines and a solar array with a floating steel fish-farming cage is proposed. The multi-function steel cage is not only for fish cultivation but also serves as the floating foundation. VAWTs are selected as the turbine architecture due to their structural simplicity, robustness, lower CG than VAWTs, and the lower wake effect, allowing them to be arranged in a compact pattern to improve the economy of the wind farm. In addition, the solar array is included as complementary power generation without compromising the wind efficiency. Thus, the concept is able to make full use of the ocean space and water resources. Moreover, the WSA system is unconditionally stable since its CG is lower than CB. Installations of all VAWTs and the solar array can be finished on the dock and then transported to operation site by wet tow. The overall power generation capacity of the WSA reaches 13.52 MW (Table 2), more than twice the power of a single HAWT in the Hywind Scotland wind farm and even 63% larger than the 8.3-MW HAWT being developed in the Portugal Windfloat Atlantic wind farm.

Hydrostatic analysis at the operation draft shows that the largest deformation of only 112 mm occurs at the center of the cage. Additionally, it is found from modal analysis that the first natural frequency of vibration is 0.81 Hz, well outside the range of wave frequencies. All these demonstrate that the steel cage floater can be regarded as a rigid body for the hydrodynamic analysis. The calculated motion RAOs in the free-floating states illustrate that the heave and pitch natural periods of the WSA system are far beyond the possible wave period range. The comparison of the WSA's RAOs with the favorable OC3Hywind and OC4DeepCwind concepts demonstrates that the seakeeping performance of the WSA is better than its counterparts.

A potential operation site located in the South China Sea was selected as a case study to examine the feasibility of WSA. Time-domain simulations of dynamic responses subject to wind, waves, and current in three survival load cases were carried out. The wind and wave conditions used in the analyses were based on the dataset available from ECMWF. In the 50-year wind-dominated sea state, as well as the swell-dominated sea state, the extreme hydrodynamic motions (heave and pitch), structural dynamic responses (tower top accelerations and tower base stress of a VAWT), and mooring line tensions were all within safe ranges, while responses tended to be Gaussian with small skewness and kurtosis.

Technically, for survival conditions in which VAWTs are parked, the present study validated the WSA's technical feasibility as a multi-function floater in moderately deep seas for offshore power exploitation and marine aquaculture. The WSA, already filed in two patent applications, will become a competitive and promising design for marine aquaculture and the offshore wind power industry. Future research will be extended to the layout optimization of turbines and another extreme condition, in which VAWTs are rotating in rated speed for continuous power generation. In severe seas, for such a mega-floater, the second-order hydrodynamic effect might boost the non-Gaussianity of seakeeping motions and structural responses. The level of non-Gaussianity also needs in-depth study.

Author Contributions: Conceptualization, X.Z.; methodology, X.Z. and H.Z.; software, H.Z and Y.L. (Yu Lei); formal analysis, H.Z.; investigation, H.Z.; resources, X.Z., Y.L. (Yi Li), and W.L.; writing—original draft, H.Z.;

writing—review and editing, X.Z.; visualization, H.Z. All authors have read and agreed to the published version of the manuscript.

Funding: This research work was supported by the China National Key Research Scheme 2016YFC0303706 and the China National Science Foundation project Grant No. 51579227.

Conflicts of Interest: The authors declare no conflicts of interest.

References

1. Cahay, M.; Luquiau, E.; Smadja, C. Use of a vertical wind turbine in an offshore floating wind farm. In Proceedings of the Offshore Technology Conference, Houston, TX, USA, 2–5 May 2011.
2. Bore, P.T.; Fossan, P.A. Ultimate-and Fatigue Limit State Analysis of a Rigid Offshore Aquaculture Structure. Master’s Thesis, NTNU, Taipei, Taiwan, 2015.
3. Owano, N. Three Months Show Hywind Scotland Floating Wind Farm Exceeding Expectations. Available online: <https://techxplore.com/news/2018-02-months-hywind-scotlandfarm-exceeding.html> (accessed on 19 February 2018).
4. Dabiri, J.O. Potential order-of-magnitude enhancement of wind farm power density via counter-rotating vertical-axis wind turbine arrays. *J. Renew. Sustain. Energy* **2011**, *3*, 043104. [CrossRef]
5. Apelfröjd, S.; Eriksson, S.; Bernhoff, H. A review of research on large scale modern vertical axis wind turbines at Uppsala University. *Energies* **2016**, *9*, 570. [CrossRef]
6. Paulsen, U.S.; Pedersen, T.F.; Madsen, H.A.; Enevoldsen, K.; Hattel, J.H. Deepwind—An innovative wind turbine concept for offshore. In Proceedings of the EWEA Annual Event 2011, Bursseles, Belgium, 14–17 March 2011; European Wind Energy Association (EWEA): Bursseles, Belgium, 2011.
7. 10MW Aerogenerator X © Wind Power Limited & Grimshaw. Available online: <http://vimeo.com/13654447> (accessed on 4 May 2015).
8. Adam, F.; Myland, T.; Schuldt, B.; Großmann, J.; Dahlhaus, F. Evaluation of internal force superposition on a TLP for wind turbines. *Renew. Energy* **2014**, *71*, 271–275. [CrossRef]
9. Roddier, D.; Cermelli, C.; Aubault, A.; Weinstein, A. WindFloat: A floating foundation for offshore wind turbines. *J. Renew. Sustain. Energy* **2010**, *2*, 033104. [CrossRef]
10. Kvittem, M.I.; Bachynski, E.E.; Moan, T. Effects of hydrodynamic modelling in fully coupled simulations of a semi-submersible wind turbine. *Energy Proced.* **2012**, *24*, 351–362. [CrossRef]
11. Karimirad, M.; Michailides, C. V-shaped semisubmersible offshore wind turbine: An alternative concept for offshore wind technology. *Renew. Energy* **2015**, *83*, 126–143. [CrossRef]
12. Wen, T.; Wang, K.; Cheng, Z.; Ong, M. Spar-Type Vertical-Axis Wind Turbines in Moderate Water Depth: A Feasibility Study. *Energies* **2018**, *11*, 555. [CrossRef]
13. Karimirad, M.; Moan, T. Wave-and wind-induced dynamic response of a spar-type offshore wind turbine. *J. Waterw. Port Coast. Ocean Eng.* **2011**, *138*, 9–20. [CrossRef]
14. Zheng, X.; Lei, Y. Stochastic Response Analysis for a Floating Offshore Wind Turbine Integrated with a Steel Fish Farming Cage. *Appl. Sci.* **2018**, *8*, 1229. [CrossRef]
15. Karimirad, M. Modeling aspects of a floating wind turbine for coupled wave–wind-induced dynamic analyses. *Renew. Energy* **2013**, *53*, 299–305. [CrossRef]
16. Sethuraman, L.; Venugopal, V. Hydrodynamic response of a stepped-spar floating wind turbine: Numerical modelling and tank testing. *Renew. Energy* **2013**, *52*, 160–174. [CrossRef]
17. Duan, F.; Hu, Z.; Niedzwecki, J.M. Model test investigation of a spar floating wind turbine. *Mar. Struct.* **2016**, *49*, 76–96. [CrossRef]
18. Utsunomiya, T.; Sato, T.; Matsukuma, H.; Yago, K. Experimental validation for motion of a spar-type floating offshore wind turbine using 1/22.5 scale model. In Proceedings of the ASME 2009 28th International Conference on Ocean, Offshore and Arctic Engineering, Honolulu, HI, USA, 31 May–5 June 2009; American Society of Mechanical Engineers: New York, NY, USA, 2009; pp. 951–959.
19. Yang, H.; Wei, Z.; Chengzhi, L. Optimal design and techno-economic analysis of a hybrid solar–wind power generation system. *Appl. Energy* **2009**, *86*, 163–169. [CrossRef]
20. Zhou, W.; Lou, C.; Li, Z.; Lu, L.; Yang, H. Current status of research on optimum sizing of stand-alone hybrid solar–wind power generation systems. *Appl. Energy* **2010**, *87*, 380–389. [CrossRef]

21. Yang, H.; Lu, L.; Zhou, W. A novel optimization sizing model for hybrid solar-wind power generation system. *Solar Energy* **2007**, *81*, 76–84. [[CrossRef](#)]
22. Jonkman, J. *Definition of the Floating System for Phase IV of OC3*; NREL/TP-500-47535; National Renewable Energy Laboratory (NREL): Golden, CO, USA, 2010.
23. Robertson, A.; Jonkman, J.; Masciola, M.; Song, H.; Goupee, A.; Coulling, A.; Luan, C. *Definition of the Semisubmersible Floating System for Phase II of OC4*; NREL/TP-5000-60601; National Renewable Energy Laboratory (NREL): Golden, CO, USA, 2014.
24. Manual, O. Available online: <http://www.Orcina.com/SoftwareProducts/OrcaFlex/Documentation> (accessed on 21 November 2019).
25. Tsukrov, I.; Drach, A.; Decew, J.; Swift, M.R.; Celikkol, B. Characterization of geometry and normal drag coefficients of copper nets. *Ocean Eng.* **2011**, *38*, 1979–1988. [[CrossRef](#)]
26. Cheng, Z.; Wang, K.; Gao, Z.; Moan, T. A comparative study on dynamic responses of spar-type floating horizontal and vertical axis wind turbines. *Wind Energy* **2017**, *20*, 305–323. [[CrossRef](#)]
27. Borg, M.; Collu, M. Frequency-domain characteristics of aerodynamic loads of offshore floating vertical axis wind turbines. *Appl. Energy* **2015**, *155*, 629–636. [[CrossRef](#)]
28. Lin, J.; Xu, Y.L.; Xia, Y.; Li, C. Structural Analysis of Large-Scale Vertical-Axis Wind Turbines, Part I: Wind Load Simulation. *Energies* **2019**, *12*, 2573. [[CrossRef](#)]
29. Cheng, Z.; Madsen, H.A.; Gao, Z.; Moan, T. Effect of the number of blades on the dynamics of floating straight-bladed vertical axis wind turbines. *Renew. Energy* **2017**, *101*, 1285–1298. [[CrossRef](#)]
30. Goett, H.J.; Bullivant, W.K. *Tests of NACA 0009, 0012, and 0018 Airfoils in the Full-Scale Tunnel*; US Government Printing Office: Washington, DC, USA, 1938.
31. DNV GL. *Offshore Standard: Position Mooring*; DNVGL-OS-E301; DNV GL: Høvik, Norway, 2015.
32. Jeon, S.H.; Cho, Y.U.; Seo, M.W.; Cho, J.R.; Jeong, W.B. Dynamic response of floating substructure of spar-type offshore wind turbine with catenary mooring cables. *Ocean Eng.* **2013**, *72*, 356–364. [[CrossRef](#)]
33. Herman, S.A. *Offshore Wind Farms: Analysis of Transport and Installation Costs*; Energy Research Centre of the Netherlands: Petten, The Netherlands, 2002.
34. Ahn, D.; Shin, S.; Kim, S.; Kim, H. Comparative evaluation of different offshore wind turbine installation vessels for Korean west–south wind farm. *Int. J. Nav. Archit. Ocean Eng.* **2017**, *9*, 45–54. [[CrossRef](#)]
35. Hibbitt, H.; Karlsson, B.; Sorensen, P. *Abaqus Analysis User's Manual Version 6.10*; Dassault Systèmes Simulia Corp: Providence, RI, USA, 2011.
36. WAMIT, Inc. *WAMIT User Manual*, version 7.0; WAMIT, Inc.: Chestnut Hill, MA, USA, 2013.
37. AeroHydro, Inc. *MultiSurf User Manual*, version 8.0; AeroHydro, Inc.: Southwest Harbor, ME, USA, 2011.
38. Barltrop, N.D.P.; Adams, A.J. *Dynamics of Fixed Marine Structures*, 3rd ed.; Butterworth-Heinemann Ltd.: Oxford, UK, 1991; pp. 310–319. ISBN 978-0-7506-1046-9.
39. Cifuentes, C.; Kim, M.H. Numerical simulation of wake effect in nets under steady current. In Proceedings of the ASME 2015 34th International Conference on Ocean, Offshore and Arctic Engineering, Newfoundland, NL, Canada, 31 May–5 June 2015; American Society of Mechanical Engineers: New York, NY, USA, 2015.
40. Jonkman, J.M.; Buhl, M.L., Jr. *FAST User's Guide*; Technical Report No. NREL/EL-500-38230; National Renewable Energy Laboratory: Golden, CO, USA, 2005.
41. Cummins, W.E. *The Impulse Response Function and Ship Motions*; David Taylor Model Basin: Washington, DC, USA, 1962.
42. DNV. *Recommended Practice: Environmental Conditions and Environmental Loads*; DNV-RP-C205; Det Norske Veritas: Høvik, Oslo, Norway, 2007.
43. Anagnostopoulou, C.; Kagemoto, H.; Sao, K.; Mizuno, A. Concept design and dynamic analyses of a floating vertical-axis wind turbine: Case study of power supply to offshore Greek islands. *J. Ocean Eng. Mar. Energy* **2016**, *2*, 85–104. [[CrossRef](#)]
44. American Society of Civil Engineers. *Minimum Design Loads for Buildings and Other Structures (ASCE/SEI 7-16)*; American Society of Civil Engineers: Reston, VA, USA, 2016.
45. DNV GL. *Design of Offshore Wind Turbine Structures*; DNV-OS-J101; DNV GL: Høvik, Norway, 2013.
46. European Centre for Medium-Range Weather Forecasts Public Dataset ERA Interim. Available online: <http://apps.ecmwf.int/datasets/data/interim-full-daily/levtype=sfc/> (accessed on 21 November 2019).
47. API, *Recommended Practice for Planning, Designing and Constructing Fixed Offshore Platforms—Working Stress Design*; American Petroleum Institute (API): Washington, DC, USA, 1993.

48. IEC. *IEC 61400-1, Wind Turbines-Part 1: Design Requirements*, 3rd ed.; International Electrotechnical Commission: Geneva, Switzerland, 2005.
49. Bitner-Gregersen, E.M.; Haver, S. Joint environmental model for reliability calculations. In *Proceedings of the First International Offshore and Polar Engineering Conference*, Edinburgh, UK, 11–16 August 1991; International Society of Offshore and Polar Engineers: Mountain View, CA, USA, 1991.
50. Torsethaugen, K.; Haver, S. Simplified double peak spectral model for ocean waves. In *Proceedings of the Fourteenth International Offshore and Polar Engineering Conference*, Toulon, France, 23–28 May 2004; International Society of Offshore and Polar Engineers: Mountain View, CA, USA, 2004.
51. Campanile, A.; Piscopo, V.; Scamardella, A. Mooring design and selection for floating offshore wind turbines on intermediate and deep water depths. *Ocean Eng.* **2018**, *148*, 349–360. [[CrossRef](#)]
52. DNV GL. *Coupled Analysis of Floating Wind Turbines*; DNVGL-RP-0286; DNV GL: Høvik, Norway, 2019.



© 2020 by the authors. Licensee MDPI, Basel, Switzerland. This article is an open access article distributed under the terms and conditions of the Creative Commons Attribution (CC BY) license (<http://creativecommons.org/licenses/by/4.0/>).